Proceedings of ASME Turbo Expo 2011
GT2011
June 6-10, 2011, Vancouver, British Columbia, Canada

GT2011-45788

ANALYTICAL FORCES PARAMETERS IDENTIFICATION OF HYBRID JOURNAL GAS BEARING BASED ON TRANSFER FUNCTION

Guang-hui Zhang
Harbin Institute of Technology
Harbin, Hei Longjiang Province, China

Zhan-sheng Liu
Harbin Institute of Technology
Harbin, Hei Longjiang Province, China

Gui-long Wang
Harbin Institute of Technology
Harbin, Hei Longjiang Province, China

Jia-jia Yan
Harbin Institute of Technology
Harbin, Hei Longjiang Province, China

ABSTRACT

A mathematical model for the flow in the hybrid gas journal bearing is depicted by the transfer function in this paper. The average and modified parameters from the pressure distribution of multi-orifices aerostatic journal bearing are acquired to describe the characteristics accurately. The transient gas film forces of multi-orifices hybrid bearing is derived in the generalized form by analytical means, and then the dynamic characteristics coefficients are got by employing the Laplace transform. It indicates that the obtained forces can calculate the dynamic characteristics coefficients simply, quickly and accurately, which provide an efficient means for designing rotor-bearing systems.

NOMENCLATURE

h_m	average film thickness of the bearing
k_a	average pressure distribution parameter along the length of the bearing
k_h	average parameter of bearing clearance cause by changes of journal motion
k_L	zone length parameter
k_θ	average pressure distribution parameter along the circumferential direction θ of the bearing
l	the length of the bearing
p^*	pressure of the bearing for midline of the bearing
p_0	$p_0 = k_s\left(p_c - p_a\right) + p_a$
$\overline{P}_0$	dimensionless form of p_0,
p_a	atmosphere pressure
$\overline{p}_c$	dimensionless downstream pressure at orifices
p_m	average pressure in bearing zone $p_m = k_a\left(p_0 - p_a\right) + p_a$
$\overline{p}_m$	dimensionless average pressure in bearing zone
p_m^*	pressure distribution parameter of bearing for circumferential direction
p_m^{**}	pressure distribution parameter of bearing for the length direction
$p_{m\max}^*$	the maximum pressure of p_m^*
p_{qm}^*	the square average pressure parameters
p_s	supply pressure for hybrid gas bearing
$\overline{p}_s$	dimensionless supply pressure
Δp	pressure increment at the center point of the selected zone
Δp_0	average pressure increment in the middle plane $\Delta p_0 = k_\theta \Delta p$
Δp_m	average pressure increment for the bearing zone $\Delta p_m = k_a k_\theta \Delta p$
q	mass flow rate of gas
s	$i\omega_f$, $i = \sqrt{-1}$
$\overline{s}$	$i\overline{\omega}$
Δy	shaft displacement in the y direction
$A_{orifice}$	the area of the orifice
D	diameter of the bearing
$\Delta\overline{F}_x, \Delta\overline{F}_y$	dimensionless gas film forces on the shaft

L	the length of the bearing
L^*	the length of the zones for bearing circumferential direction
R	the radius of the bearing
R^0	gas constant
T^0	absolute temperature
W_{xy}, W_{yy}	transfer function of bearing
θ	angular coordinate
μ	dynamic viscosity
ρ_a	gas density
$\phi_{orifice}$	flow restriction parameter for orifices
ψ_i	flow function of the i th orifices
ω	angular velocity
$\bar{\omega}$	dimensionless frequency
ω_f	frequency
Λ	dimensionless bearing number $(6\mu\omega/p_a)(R/h_m)^2$

INTRODUCTION

The gas bearings are widely used in mechanical and aerospace engineering for their less friction and high rotating speeds. The aerodynamic and aerostatic effect are coupled together to generate the load capacity for the hybrid gas bearing. So the wear of the self-acting bearing during the start and coasting down is avoided. The hybrid gas bearings are employed in more application for more improved stability than that of self-acting bearing and higher stiffness than that of aerostatic bearing. It is significant to obtain the damping and stiffness coefficients which are the important design parameters for hybrid gas bearings.

There are two ways to study the dynamic characteristics of gas bearing theoretically. One way is solving the gas lubricated Reynolds equation by analytical method, and the formula of gas film force is employed to depict the dynamic characteristics of gas bearing. Some of early researches neglected the pressure derivation with respect to time as the simplified means. The resulting quasi-static solution are quite satisfactory for incompressible lubrication, but cannot represent the physical property of gas lubricated film, so this method is only fitted for the cases of lower rotating speeds[1,2]. Based on the previous work, the linearized technique is employed to develop the modified analytical method considering the time term [3, 4]. Generally speaking, the analytical solution of gas lubricated Reynolds equation is hard to obtain without simplification. The other means is solving the gas lubricated Reynolds equation by numerical simulation to get the stiffness and damping coefficients [5, 6]. Carpino[7] employed the finite element foil bearing model and the perturbation means to analyze the rotor dynamic coefficients. Also the energy dissipation rate for the bearing was presented in the paper. Mihai Arghir[8] adopted the finite element modeling of a bump-type foil-bearing structure and studied its static and dynamic behavior under different load cases. San Andres [9] used a bulk flow model to predict rotor dynamic coefficients for a foil bearing with turbulent flows. Lee, et al.[10] predicted rotor dynamic coefficients for a gas-lubricated foil journal bearing with the slip flow. M.T.C. Faria, et al.[11] analyze the high-speed hydrodynamic gas bearing using both finite element and finite difference methods. The frequency-dependent force coefficients are calculated by the perturbation method. Stefano Morosi[12] presented a detailed mathematical modeling of the gas bearing based on the compressible form of the Reynolds equation. Perturbation theory is applied in order to identify the dynamic characteristic of the bearing. The evaluation of the linearized gas-film forces coefficients for gas bearings presents a difficult problem considering that the coefficients are functions of vibration frequency. Also the main modern-day method bases on the numerical integration of the Reynolds equation.

Another way to solve the stability problem of gas bearing-rotor system is the orbit method, which is proposed by Castelli in Ref[13]. In the orbit method, the complete nonlinear equations are included, the calculation procedures highly coincide with the assumed governing equations, and the trajectory orbit of the rotor can be obtained. So the orbit method enables both establishment of the stability threshold and prediction of the behavior of the bearing into the instability region. Because of the advantages as mentioned above, the orbit method is more and more widely employed. Castelli discussed the numerical method for solving the transient Reynolds equation in Ref [14]. The proposed method possessed the satisfactory numerical stability of implicit arithmetic and the fast convergence of the explicit method. In Ref. [15] Dimofte modified the alternating direction implicit method and developed the code for analyzing the steady and dynamic characteristics. Bou-Sa solved the nonlinear Reynold equation with time terms to simulate the dynamic characteristics of the rotor in Ref[16]. The proposed model was compared with conventional linear journal bearing model which employing the stiffness and damping coefficients. It indicated that the linear model would lead to the incorrect answers; the nonlinear model could forecast the rotor dynamic characteristics better. In Ref[17], the gas lubricated Reynolds equation with time term was solved by employing the finite difference method and over relaxation method. The dynamic behavior on horizontal and vertical direction of the journal was analyzed by locus diagram, Poincare map, power spectrum and bifurcation diagram. The concept of whirling ratio was imported in the solving procedure. But the orbit method is time consuming and the effectiveness is lower.

In the Ref [18] the dynamic characteristics coefficients for self-acting gas bearing based on the transfer function are presented. The dynamic coefficients of externally pressurized gas bearing with four orifices are obtained based on that method [19]. The transfer function method mentioned above has the advantage of fast calculating speed, high efficiency and

the clear analytical form of the bearing forces. But the essence of the transfer function is a linear methods, so some limitations exist as follow: it is impossible to analyze the comprehensive nonlinear behavior of gas bearing-rotor system including the Poincare map and bifurcation characteristics; the efficiency can only be presented for a given rotor dynamic problem such as the unbalance response or stability. In Ref [19] the specificity on symmetry of the four calculation domain is employed and the deriving procedure is simplified. Based on the mentioned method, a more generalized means for acquiring the dynamic characteristics coefficients of gas bearing is proposed by using the transfer function to describe the flow between the clearances. Different from the deriving procedure in Ref.[18], the bearing clearance can be divided into arbitrary zones, without curving up the unique four calculation zone. The eight orifices externally pressurized gas bearing is analyzed as an instance and the analytical form of gas film forces is acquired. Finally the stiffness and damping coefficients for eight orifices externally pressurized gas bearing are obtained in this paper, which provide a compact and effective method for the dynamic analysis of gas bearings.

1 DEPICTION FOR FLOW IN CLEARANCE

The physical models for two typical journal gas bearing are presented: (1) self-acting gas bearing; (2) externally pressurized hybrid gas bearing (eight orifices which located in the middle line of the bearing).

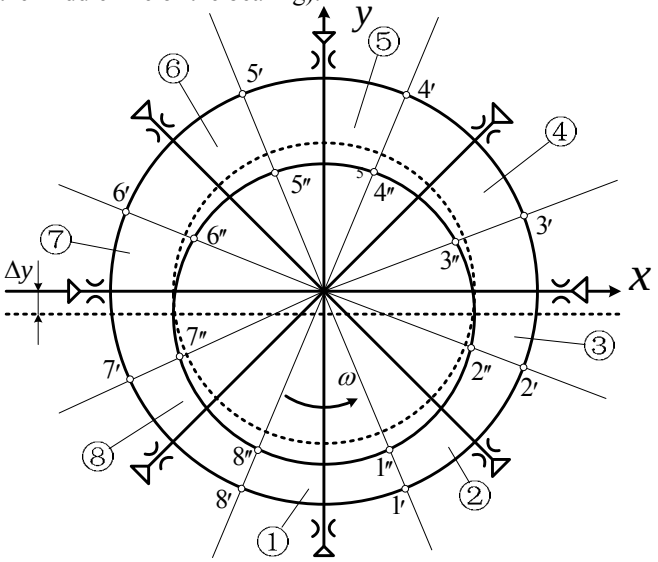

Figure.1 Schematic diagram of the center plane of the hybrid gas journal bearing

A schematic diagram of the center plane of an externally pressurized journal bearing with coordinate system is shown in Fig.1. The clearance between the shaft and the bearing is divided into eight zones. The coordinate x, y-axes are fixed to the bearing with the origin at the bearing center and pass through the centers of the zones where the orifices are disposed. The eight orifices located on the x, y axes, and the axes with 45 degreed angels between each other. The vertical downward displacement in the y direction -△y is taken as the input signal. The shaft rotates anticlockwise with angular velocity ω. The mass flow conservation equation for zone ① is presented as follows:

$$q_8 - q_1 - q_{12} - q_{18} - q_{a1} + q_{s1} - q_{d1} = 0 \tag{1}$$

Where q_8, q_1 are the mass flow rates of gas in the θ direction produced by the rotating of the shaft in the section $8'-8''$ and $1'-1''$ respectively; q_{12}, q_{18} are the mass flow rates of gas in the θ direction generated from the pressure differences in zone①, ② and zone ①, ⑧ respectively; q_{a1} is the mass flow rates in the axes z direction produced by the pressure differences in zone ① and the environment pressure; q_{s1} is the mass flow rated produced by the externally pressurized orifices; q_{d1} is the dynamic flow mass rated generated from the motion of the shaft in zone①.

1.1 SIMPLIFIED ASSUMPTION

For the procedure of modeling with transfer function, several assumptions are presented: the flow in the bearing clearance is isothermal and perfect gas law can be employed; the velocity distribution in the bearing clearance produced by the rotation of the shaft is linear; the velocity distribution produced by the pressure difference is parabolic; the clearance of the bearing is much less than the radius of the bearing; the diameter of the orifice is negligibly small relative to the bearing radius.

By employing the method proposed in Ref [19], several assumptions are employed to simplify the model as follows:

1 In the present model we work with averaged uniform initial level pressure distributions in the θ-direction defined for the center plane of the bearing as: $p_0 = k_s\left(p_c - p_a\right) + p_a$. In the z-direction beginning at the center plane a decrease of averaged pressure from the pressure level p_0 to ambient pressure p_a takes place. We can write the average mean pressure level for the zones as: $p_m = k_a\left(p_0 - p_a\right) + p_a$.

2 For each zone we define: Δp is the increment pressure in the center of zones; $\Delta p_0 = k_\theta \Delta p$ is the average increment pressure in the zone center plane; $\Delta p_m = k_a k_\theta \Delta p$ is the average increment pressure in zone.

3 At the boundaries between the zones in the center plane of the bearing we assume the increment pressure as the mean value between the increment pressures in the center plane of adjacent zones. For example, at the boundary between zones 1 and 2 in the center plane the increment pressure can be written as: $\Delta p_{1'-1''} = 0.5\times\left(\Delta p_1 + \Delta p_2\right)$. In this case for the average increment pressure at the boundary we can write $k_a \Delta p_{1'-1''} = 0.5 k_a\left(\Delta p_1 + \Delta p_2\right)$.

1.2 MATHEMATICAL MODEL OF THE FLOW

Take the zone ① as the instance, on the basis the components of Eq.(1) may be written in the following form:

1. The mass flow rates of gas in the θ direction produced by the rotating of the shaft in the section $8'-8''$ and $1'-1''$ respectively are presented as Eq. (2):

$$\begin{aligned} q_8 &= \frac{\left\{k_a\left[0.5\left(\Delta p_1+\Delta p_8\right)+p_0-p_a\right]+p_a\right\}}{R^0T^0}\times\frac{\omega R}{2}\times l\times\left(h_m-\frac{\sqrt{2+\sqrt{2}}}{2}\Delta y\right) \\ q_1 &= \frac{\left\{k_a\left[0.5\left(\Delta p_1+\Delta p_2\right)+p_0-p_a\right]+p_a\right\}}{R^0T^0}\times\frac{\omega R}{2}\times l\times\left(h_m-\frac{\sqrt{2+\sqrt{2}}}{2}\Delta y\right) \end{aligned} \tag{2}$$

2. The mass flow rates of gas in the θ direction generated from the pressure differences in zone①, ② and zone ①, ⑧ respectively are presented as Eq.(3):

3. the mass flow rates in the axes z direction produced by the pressure differences in zone ① and the environment pressure is presented as Eq.(4):

$$\begin{aligned} q_{12} &= \frac{\left(h_m-\left(\sqrt{2+\sqrt{2}}/2\right)\Delta y\right)^3\times l}{24\mu R^0T^0L^*}\left\{\left[k_a\left(p_0+\Delta p_1-p_a\right)+p_a\right]^2-\left[k_a\left(p_0+\Delta p_2-p_a\right)+p_a\right]^2\right\} \\ q_{18} &= \frac{\left(h_m-\left(\sqrt{2+\sqrt{2}}/2\right)\Delta y\right)^3\times l}{24\mu R^0T^0L^*}\left\{\left[k_a\left(p_0+\Delta p_1-p_a\right)+p_a\right]^2-\left[k_a\left(p_0+\Delta p_8-p_a\right)+p_a\right]^2\right\} \end{aligned} \tag{3}$$

$$q_{a1} = \frac{\left(h_m-k_h\Delta y\right)^3 4L^*}{24\mu R^0T^0l}\left[\left(p_0+k_\theta\Delta p_1\right)^2-p_a^2\right] \tag{4}$$

4. the mass flow rate produced by the externally pressurized orifices[20] is presented as Eq.(5):

5. the dynamic flow mass rate generated from the motion of the shaft in zone① is presented as Eq.(6):

$$q_{s1} = \phi_{orifice}\,p_s A_{orifice}\sqrt{\frac{2\rho_a}{p_a}}\psi_i = \phi_{orifice}\,p_s A_{orifice}\sqrt{2}\left(R_0T_0\right)^{-0.5}\psi_i \tag{5}$$

$$q_{d1} = \frac{L^*l}{R^0T^0}\frac{d}{dt}\left\{\left(h_m-k_h\Delta y\right)\left[k_a\left(p_0+k_\theta\Delta p_1-p_a\right)+p_a\right]\right\} \tag{6}$$

Multiplying the Eq. (1) with $4R^0T^0/\left(h_m\omega Rlp_a\right)$, and then the mass flow conservation is linearized by neglecting the high order term:

Take into account for the average film thickness in different zones, the mass flow conservation equations are presented as follows:

For zone①

$$k_a\left(\Delta\bar{p}_8-\Delta\bar{p}_2\right)-\frac{2k_a\bar{p}_m}{k_L\Lambda}\left(2\Delta\bar{p}_1-\Delta\bar{p}_2-\Delta\bar{p}_8\right)-\frac{2k_Lk_\theta\bar{p}_0}{a^2\Lambda}\Delta\bar{p}_1-\frac{k_L}{a^2\Lambda}\left(\bar{p}_0^2-1\right)+\frac{c_f}{c_c\Lambda}\Delta\bar{p}_1-2Tk_Lk_ak_\theta\frac{d\Delta\bar{p}_1}{dt}+2Tk_hk_L\bar{p}_m\frac{d\Delta\bar{y}}{dt}=0 \tag{7}$$

For zone②:

$$k_a\left(\Delta\bar{p}_1-\Delta\bar{p}_3\right)+\frac{1}{\sqrt{2+\sqrt{2}}}\bar{p}_m\Delta\bar{y}-\frac{2k_a\bar{p}_m}{k_L\Lambda}\left(2\Delta\bar{p}_2-\Delta\bar{p}_1-\Delta\bar{p}_3\right)-\frac{2k_Lk_\theta\bar{p}_0}{a^2\Lambda}\Delta\bar{p}_2-\frac{k_L}{a^2\Lambda}\left(\bar{p}_0^2-1\right)+\frac{3k_Lk_h\left(\bar{p}_0^2-1\right)}{a^2\Lambda}\Delta\bar{y}+\frac{c_f}{c_c\Lambda}\Delta\bar{p}_2 \tag{8}$$

$$-2Tk_L k_a k_\theta \frac{d\Delta\bar{p}_2}{dt} + 2Tk_h k_L \bar{p}_m \frac{d\Delta\bar{y}}{dt} = 0$$

For zone③:

$$k_a\left(\Delta\bar{p}_2 - \Delta\bar{p}_4\right) + \frac{\sqrt{2}}{\sqrt{2+\sqrt{2}}}\bar{p}_m\Delta\bar{y} - \frac{2k_a\bar{p}_m}{k_L\Lambda}\left(2\Delta\bar{p}_3 - \Delta\bar{p}_2 - \Delta\bar{p}_4\right) - \frac{2k_L k_\theta \bar{p}_0}{a^2\Lambda}\Delta\bar{p}_3 - \frac{k_L}{a^2\Lambda}\left(\bar{p}_0^2 - 1\right) + \frac{3k_L k_h\left(\bar{p}_0^2 - 1\right)}{a^2\Lambda}\Delta\bar{y}$$
$$+ \frac{c_f}{c_c\Lambda}\Delta\bar{p}_3 - 2Tk_L k_a k_\theta \frac{d\Delta\bar{p}_3}{dt} + 2Tk_h k_L \bar{p}_m \frac{d\Delta\bar{y}}{dt} = 0 \tag{9}$$

For zone④:

$$k_a\left(\Delta\bar{p}_3 - \Delta\bar{p}_5\right) - \frac{1}{\sqrt{2+\sqrt{2}}}\bar{p}_m\Delta\bar{y} - \frac{2k_a\bar{p}_m}{k_L\Lambda}\left(2\Delta\bar{p}_4 - \Delta\bar{p}_3 - \Delta\bar{p}_5\right) - \frac{2k_L k_\theta \bar{p}_0}{a^2\Lambda}\Delta\bar{p}_4$$
$$- \frac{k_L}{a^2\Lambda}\left(\bar{p}_0^2 - 1\right) - \frac{3k_L k_h\left(\bar{p}_0^2 - 1\right)}{a^2\Lambda}\Delta\bar{y} + \frac{c_f}{c_c\Lambda}\Delta\bar{p}_4 - 2Tk_L k_a k_\theta \frac{d\Delta\bar{p}_4}{dt} - 2Tk_h k_L \bar{p}_m \frac{d\Delta\bar{y}}{dt} = 0 \tag{10}$$

For zone⑤:

$$k_a\left(\Delta\bar{p}_4 - \Delta\bar{p}_6\right) - \frac{2k_a\bar{p}_m}{k_L\Lambda}\left(2\Delta\bar{p}_5 - \Delta\bar{p}_4 - \Delta\bar{p}_6\right) - \frac{2k_L k_\theta \bar{p}_0}{a^2\Lambda}\Delta\bar{p}_5 - \frac{k_L}{a^2\Lambda}\left(\bar{p}_0^2 - 1\right)$$
$$- \frac{3k_L k_h\left(\bar{p}_0^2 - 1\right)}{a^2\Lambda}\Delta\bar{y} + \frac{c_f}{c_c\Lambda}\Delta\bar{p}_5 - 2Tk_L k_a k_\theta \frac{d\Delta\bar{p}_5}{dt} - 2Tk_h k_L \bar{p}_m \frac{d\Delta\bar{y}}{dt} = 0 \tag{11}$$

For zone⑥:

$$k_a\left(\Delta\bar{p}_5 - \Delta\bar{p}_7\right) - \frac{1}{\sqrt{2+\sqrt{2}}}\bar{p}_m\Delta\bar{y} - \frac{2k_a\bar{p}_m}{k_L\Lambda}\left(2\Delta\bar{p}_6 - \Delta\bar{p}_5 - \Delta\bar{p}_7\right) - \frac{2k_L k_\theta \bar{p}_0}{a^2\Lambda}\Delta\bar{p}_6$$
$$- \frac{k_L}{a^2\Lambda}\left(\bar{p}_0^2 - 1\right) - \frac{3k_L k_h\left(\bar{p}_0^2 - 1\right)}{a^2\Lambda}\Delta\bar{y} + \frac{c_f}{c_c\Lambda}\Delta\bar{p}_6 - 2Tk_L k_a k_\theta \frac{d\Delta\bar{p}_6}{dt} - 2Tk_h k_L \bar{p}_m \frac{d\Delta\bar{y}}{dt} = 0 \tag{12}$$

For zone⑦:

$$k_a\left(\Delta\bar{p}_6 - \Delta\bar{p}_8\right) + \frac{\sqrt{2}}{\sqrt{2+\sqrt{2}}}\bar{p}_m\Delta\bar{y} - \frac{2k_a\bar{p}_m}{k_L\Lambda}\left(2\Delta\bar{p}_7 - \Delta\bar{p}_6 - \Delta\bar{p}_8\right) - \frac{2k_L k_\theta \bar{p}_0}{a^2\Lambda}\Delta\bar{p}_7$$
$$- \frac{k_L}{a^2\Lambda}\left(\bar{p}_0^2 - 1\right) + \frac{3k_L k_h\left(\bar{p}_0^2 - 1\right)}{a^2\Lambda}\Delta\bar{y} + \frac{c_f}{c_c\Lambda}\Delta\bar{p}_7 - 2Tk_L k_a k_\theta \frac{d\Delta\bar{p}_7}{dt} + 2Tk_h k_L \bar{p}_m \frac{d\Delta\bar{y}}{dt} = 0 \tag{13}$$

For zone⑧:

$$k_a\left(\Delta\bar{p}_7 - \Delta\bar{p}_1\right) + \frac{1}{\sqrt{2+\sqrt{2}}}\bar{p}_m\Delta\bar{y} - \frac{2k_a\bar{p}_m}{k_L\Lambda}\left(2\Delta\bar{p}_8 - \Delta\bar{p}_7 - \Delta\bar{p}_1\right) - \frac{2k_L k_\theta \bar{p}_0}{a^2\Lambda}\Delta\bar{p}_8$$
$$- \frac{k_L}{a^2\Lambda}\left(\bar{p}_0^2 - 1\right) + \frac{3k_L k_h\left(\bar{p}_0^2 - 1\right)}{a^2\Lambda}\Delta\bar{y} + \frac{c_f}{c_c\Lambda}\Delta\bar{p}_8 - 2Tk_L k_a k_\theta \frac{d\Delta\bar{p}_8}{dt} + 2Tk_h k_L \bar{p}_m \frac{d\Delta\bar{y}}{dt} = 0 \tag{14}$$

2. NONLINEAR GAS FILM FORCES WITH ANALYTICAL FORM

By subtracting Eq. (7) from Eq. (11), subtracting Eq. (8) from Eq. (12), subtracting Eq. (9) from Eq. (13), subtracting Eq. (12) from Eq. (14), and the variations are defined as follows: $\Delta\bar{p}_{x1} = \Delta\bar{p}_7 - \Delta\bar{p}_3$, $\Delta\bar{p}_{y1} = \Delta\bar{p}_1 - \Delta\bar{p}_5$, $\Delta\bar{p}_{x2} = \frac{\sqrt{2}}{2}\Delta\bar{p}_6 - \frac{\sqrt{2}}{2}\Delta\bar{p}_2$, $\Delta\bar{p}_{y2} = \frac{\sqrt{2}}{2}\Delta\bar{p}_2 - \frac{\sqrt{2}}{2}\Delta\bar{p}_6$, $\Delta\bar{p}_{x3} = \frac{\sqrt{2}}{2}\Delta\bar{p}_8 - \frac{\sqrt{2}}{2}\Delta\bar{p}_4$, $\Delta\bar{p}_{y3} = \frac{\sqrt{2}}{2}\Delta\bar{p}_8 - \frac{\sqrt{2}}{2}\Delta\bar{p}_4$.

And then the following equation is as follows:

$$\sqrt{2}k_a\left(\Delta\bar{p}_{x3}+\Delta\bar{p}_{x2}\right)-\frac{2k_a\bar{p}_m}{k_L\Lambda}\left(2\Delta\bar{p}_{y1}+\sqrt{2}\Delta\bar{p}_{x2}-\sqrt{2}\Delta\bar{p}_{x3}\right)-\frac{2k_Lk_\theta\bar{p}_0}{a^2\Lambda}\Delta\bar{p}_{y1}+\frac{6k_Lk_h\left(\bar{p}_0^2-1\right)}{a^2\Lambda}\Delta\bar{y}+\frac{c_f}{c_c\Lambda}\Delta\bar{p}_{y1}$$
$$-2Tk_Lk_ak_\theta\frac{d\Delta\bar{p}_{y1}}{dt}+4Tk_hk_L\bar{p}_m\frac{d\Delta\bar{y}}{dt}=0 \tag{15}$$

$$k_a\left(\Delta\bar{p}_{y1}+\Delta\bar{p}_{x1}\right)+\frac{2}{\sqrt{2+\sqrt{2}}}\bar{p}_m\Delta\bar{y}-\frac{2k_a\bar{p}_m}{k_L\Lambda}\left(2\sqrt{2}\Delta\bar{p}_{y2}-\Delta\bar{p}_{y1}+\Delta\bar{p}_{x1}\right)-\frac{2\sqrt{2}k_Lk_\theta\bar{p}_0}{a^2\Lambda}\Delta\bar{p}_{y2}+\frac{6k_Lk_h\left(\bar{p}_0^2-1\right)}{a^2\Lambda}\Delta\bar{y}+\frac{c_f}{c_c\Lambda}\sqrt{2}\Delta\bar{p}_{y2}$$
$$-2\sqrt{2}Tk_Lk_ak_\theta\frac{d\Delta\bar{p}_{y2}}{dt}+4Tk_hk_L\bar{p}_m\frac{d\Delta\bar{y}}{dt}=0 \tag{16}$$

$$\sqrt{2}k_a\left(\Delta\bar{p}_{y2}+\Delta\bar{p}_{y3}\right)-\frac{2k_a\bar{p}_m}{k_L\Lambda}\left(-2\Delta\bar{p}_{x1}+\sqrt{2}\Delta\bar{p}_{x2}+\sqrt{2}\Delta\bar{p}_{x3}\right)+\frac{2k_Lk_\theta\bar{p}_0}{a^2\Lambda}\left(\Delta\bar{p}_{x1}\right)-\frac{c_f}{c_c\Lambda}\left(\Delta\bar{p}_{x1}\right)+2Tk_Lk_ak_\theta\frac{d\left(\Delta\bar{p}_{x1}\right)}{dt}=0 \tag{17}$$

$$k_a\left(-\Delta\bar{p}_{x1}+\Delta\bar{p}_{y1}\right)-\frac{2}{\sqrt{2+\sqrt{2}}}\bar{p}_m\Delta\bar{y}-\frac{2k_a\bar{p}_m}{k_L\Lambda}\left(-2\sqrt{2}\Delta\bar{p}_{x3}+\Delta\bar{p}_{x1}+\Delta\bar{p}_{y1}\right)+\frac{2\sqrt{2}k_Lk_\theta\bar{p}_0}{a^2\Lambda}\left(\Delta\bar{p}_{x3}\right)-\frac{6k_Lk_h\left(\bar{p}_0^2-1\right)}{a^2\Lambda}\Delta\bar{y}-\frac{\sqrt{2}c_f}{c_c\Lambda}\left(\Delta\bar{p}_{x3}\right)$$
$$+2\sqrt{2}Tk_Lk_ak_\theta\frac{d\left(\Delta\bar{p}_{x3}\right)}{dt}-4Tk_hk_L\bar{p}_m\frac{d\Delta\bar{y}}{dt}=0 \tag{18}$$

By employing the Laplace transforming to Eq. (15), Eq. (16), Eq. (17), Eq. (18), and then add the Eq. (16) with Eq. (18), subtract the Eq. (16) from Eq. (18), and then the following equations are as follows:

$$\Delta\bar{p}_{x2}(s)+\Delta\bar{p}_{x3}(s)=\frac{-\sqrt{2}k_a\Delta\bar{p}_{y1}(s)+\frac{2\sqrt{2}k_a\bar{p}_m}{k_L\Lambda}\Delta\bar{p}_{x1}(s)}{\left(\frac{4k_a\bar{p}_m}{k_L\Lambda}+\frac{2k_Lk_\theta\bar{p}_0}{a^2\Lambda}-\frac{c_f}{c_c\Lambda}+2Tk_Lk_ak_\theta s\right)} \tag{19}$$

$$\Delta\bar{p}_{x2}(s)-\Delta\bar{p}_{x3}(s)=-\frac{\sqrt{2}k_a\Delta\bar{p}_{x1}(s)+\frac{2\sqrt{2}k_a\bar{p}_m}{k_L\Lambda}\Delta\bar{p}_{y1}(s)}{\left(\frac{4k_a\bar{p}_m}{k_L\Lambda}+\frac{2k_Lk_\theta\bar{p}_0}{a^2\Lambda}-\frac{c_f}{c_c\Lambda}+2Tk_Lk_ak_\theta s\right)}-\frac{\left(\frac{2\sqrt{2}}{\sqrt{2+\sqrt{2}}}\bar{p}_m+\frac{6\sqrt{2}k_Lk_h\left(\bar{p}_0^2-1\right)}{a^2\Lambda}+4\sqrt{2}Tk_hk_L\bar{p}_ms\right)\Delta\bar{y}(s)}{\left(\frac{4k_a\bar{p}_m}{k_L\Lambda}+\frac{2k_Lk_\theta\bar{p}_0}{a^2\Lambda}-\frac{c_f}{c_c\Lambda}+2Tk_Lk_ak_\theta s\right)} \tag{20}$$

The total gas film pressure is as follows:

$\Delta\bar{p}_x=\Delta\bar{p}_{x1}+\Delta\bar{p}_{x3}+\Delta\bar{p}_{x2}$, $\Delta\bar{p}_y=\Delta\bar{p}_{y1}-\Delta\bar{p}_{x2}+\Delta\bar{p}_{x3}$

And then the dimensionless gas film forces acted on the shaft are presented:

$\Delta\bar{F}_x=k_ak_\theta\Delta\bar{p}_x/\sqrt{2}$; $\Delta\bar{F}_x=k_ak_\theta\Delta\bar{p}_x/\sqrt{2}$

Where the $\Delta\bar{p}_x$ and $\Delta\bar{p}_y$ are presented in Eq.(21):

$$\Delta\bar{p}_x=\left\{\left[D_3(s)-D_1(s)-D_2(s)\right]-C(s)\left[D_4(s)+D_5(s)-D_6(s)\right]+\frac{\sqrt{2}k_L\Lambda}{8\bar{p}_mA}F(s)\right\}\Delta\bar{y}(s)$$
$$\Delta\bar{p}_y=\left\{C(s)\left[D_1(s)+D_2(s)-D_3(s)\right]-D_4(s)-D_5(s)+D_6(s)+D_7(s)\right\}\Delta\bar{y}(s) \tag{21}$$

The denotations are listed in Table.1.

Table1 definition list for hybrid gas bearing gas film forces based on the transfer function

notation	expression
$A(s)$	$\frac{4k_a\overline{p}_m}{k_L\Lambda}+\frac{2k_Lk_\theta\overline{p}_0}{a^2\Lambda}-\frac{c_f}{c_c\Lambda}+2Tk_Lk_ak_\theta s$
$C(s)$	$\frac{k_L\Lambda}{4\overline{p}_m}-\frac{\overline{p}_m}{k_L\Lambda}+\frac{k_L\Lambda A(s)^2}{8k_a^2\overline{p}_m}$
$B(s)$	$\frac{8k_a^2\overline{p}_m}{k_L\Lambda A(s)}-E(s)C(s)$
$E(s)$	$\frac{8(k_a\overline{p}_m)^2}{(k_L\Lambda)^2A(s)}-\frac{2k_a^2}{A(s)}-A(s)$
$F(s)$	$\frac{4}{\sqrt{2+\sqrt{2}}}\overline{p}_m+\frac{12k_Lk_h(\overline{p}_0^2-1)}{a^2\Lambda}+8Tk_hk_L\overline{p}_ms$
$D_1(s)$	$\left(1+\frac{2\sqrt{2}k_a\overline{p}_m}{k_L\Lambda A(s)}\right)\left(\frac{6k_Lk_h(\overline{p}_0^2-1)}{a^2\Lambda B(s)}+\frac{4Tk_hk_L\overline{p}_ms}{B(s)}\right)$
$D_2(s)$	$\frac{2k_a\overline{p}_m}{k_L\Lambda A(s)B(s)}\left(1+\frac{2\sqrt{2}k_a\overline{p}_m}{k_L\Lambda A(s)}\right)F(s)$
$D_3(s)$	$\frac{k_L\Lambda}{8k_a\overline{p}_mB(s)}\left(1+\frac{2\sqrt{2}k_a\overline{p}_m}{k_L\Lambda A(s)}\right)E(s)F(s)$
$D_4(s)$	$\frac{\sqrt{2}k_a}{A(s)}\left(\frac{6k_Lk_h(\overline{p}_0^2-1)}{a^2\Lambda B(s)}+\frac{4Tk_hk_L\overline{p}_ms}{B(s)}\right)$
$D_5(s)$	$\frac{2\sqrt{2}(k_a)^2\overline{p}_m}{k_L\Lambda A(s)^2B(s)}F(s)$
$D_6(s)$	$\frac{\sqrt{2}k_L\Lambda}{8\overline{p}_mA(s)B(s)}E(s)F(s)$
$D_7(s)$	$\frac{1}{A(s)}\left(\frac{2\sqrt{2}}{\sqrt{2+\sqrt{2}}}\overline{p}_m+2\sqrt{2}\times\frac{3k_Lk_h(\overline{p}_0^2-1)}{a^2\Lambda}+4\sqrt{2}Tk_hk_L\overline{p}_ms\right)-\frac{k_L\Lambda}{8k_a\overline{p}_m}\left(1+\frac{2\sqrt{2}k_a\overline{p}_m}{k_L\Lambda A(s)}\right)F(s)$

From the detail derived procedure, it is obviously that no specificity on symmetry of the calculation domain is employed. So the more generalized deducing method is proposed in this paper. For the generalized means, several key issues should be noticed:

1. for different dividing zone numbers, the average film thickness is different, which should be identified by the geometry of the zone;
2. after the mass flow conservation equations are obtained, the equation of different zones should subtract from the zones of corresponding opposite direction;
3. before the Laplace transforming, the equations should be simplified by defining the pressure difference of each double opposite zones.

3. THE DYNAMIC COEFFICIENTS OF JOURNAL GAS BEARING

From the definition of the transfer function, the dynamic characteristics with transfer form are shown in Eq.(22):

$$W_{xy}(s)=\frac{\Delta\bar{F}_x(s)}{\Delta\bar{y}(s)}=\left[D_3(s)-D_1(s)-D_2(s)\right]-C(s)\left[D_4(s)+D_5(s)-D_6(s)\right]+\frac{\sqrt{2}k_L\Lambda}{8\bar{p}_m A}F(s)$$
$$W_{yy}(s)=\frac{\Delta\bar{F}_y(s)}{\Delta\bar{y}(s)}=C(s)\left[D_1(s)+D_2(s)-D_3(s)\right]-D_4(s)-D_5(s)+D_6(s)+D_7(s) \quad (22)$$

By denoting the dimensionless frequency $\bar{\omega}=\omega_f T$ and $\bar{s}=\bar{\omega}i$, the transfer function are presented.

$$\bar{W}_{xy}(\bar{s})=\frac{\Delta\bar{F}_x(\bar{s})}{\Delta\bar{y}(\bar{s})},\ \bar{W}_{yy}(\bar{s})=\frac{\Delta\bar{F}_y(\bar{s})}{\Delta\bar{y}(\bar{s})} \quad (23)$$

Separating the real and imaginary parts of the transfer function, we can write:

$$\bar{G}_{xy}(\bar{\omega})=\sqrt{\mathrm{Re}_{xy}^2(\bar{\omega})+\mathrm{Im}_{xy}^2(\bar{\omega})} \quad (24)$$

$$\Phi_{xy}(\bar{\omega})=arctg\left(\frac{\mathrm{Im}_{xy}(\bar{\omega})}{\mathrm{Re}_{xy}(\bar{\omega})}\right) \quad (25)$$

$$\bar{G}_{yy}(\bar{\omega})=\sqrt{\mathrm{Re}_{yy}^2(\bar{\omega})+\mathrm{Im}_{yy}^2(\bar{\omega})} \quad (26)$$

$$\Phi_{yy}(\bar{\omega})=arctg\left(\frac{\mathrm{Im}_{yy}(\bar{\omega})}{\mathrm{Re}_{yy}(\bar{\omega})}\right) \quad (27)$$

Then the dimensionless stiffness and damping coefficients are expressed as:

$$\bar{K}_{xy}(\bar{\omega})=\bar{G}_{xy}(\bar{\omega})\cos\left(\Phi_{xy}(\bar{\omega})\right) \quad (28)$$

$$\bar{C}_{xy}(\bar{\omega})=\bar{G}_{xy}(\bar{\omega})\sin\left(\Phi_{xy}(\bar{\omega})\right)\bar{\omega}^{-1} \quad (29)$$

$$\bar{K}_{yy}(\bar{\omega})=\bar{G}_{yy}(\bar{\omega})\cos\left(\Phi_{yy}(\bar{\omega})\right) \quad (30)$$

$$\bar{C}_{yy}(\bar{\omega})=\bar{G}_{yy}(\bar{\omega})\sin\left(\Phi_{yy}(\bar{\omega})\right)\bar{\omega}^{-1} \quad (31)$$

For the central static equilibrium position of the shaft we have $\bar{W}_{yy}(\bar{s})=\bar{W}_{xx}(\bar{s})$, $\bar{W}_{xy}(\bar{s})=-\bar{W}_{yx}(\bar{s})$, this can be extended to the Eqs.(23)-(30), so the $\bar{K}_{xx}(\bar{\omega})=\bar{K}_{yy}(\bar{\omega})$, $\bar{K}_{xy}(\bar{\omega})=-\bar{K}_{yx}(\bar{\omega})$; $\bar{C}_{xy}(\bar{\omega})=\bar{C}_{yx}(\bar{\omega})$; $\bar{C}_{yy}(\bar{\omega})=\bar{C}_{xx}(\bar{\omega})$ so for the numerical analysis, only the $\bar{K}_{xy}(\bar{\omega})$, $\bar{K}_{yy}(\bar{\omega})$, $\bar{C}_{xy}(\bar{\omega})$, $\bar{C}_{xy}(\bar{\omega})$ are presented.

4. IDENTIFICATION OF THE MODIFIED PRESSURE DISTRIBUTION COEFFICIENTS

The gas film forces in each zone are depicted by defining the average parameters. The pressure distributions in circumferential direction of different section are defined by the following parameters:

$$p_m^*=\frac{1}{2\pi}\int_0^{2\pi}p^*d\theta;\ p_m^{**}=p_m^*/p_{m\max}^*$$

$p_{m\max}^*$ is the maximum value of p_m^* in the bearing length direction. The p_m^* can be employed to calculate the pressure distribution parameter k_s that located on the middle plane of the bearing along the circumferential direction; the p_m^{**} can be employed to calculate the pressure distribution parameter k_a along the length of the bearing. By applying the results of pressure distribution of hybrid gas bearing in Ref[20], and fitting the simulated pressures, we can obtain:

(1)the average parameter k_a for pressure distribution along the length of the bearing depends on the downstream pressure of orifices k_a, or $k_a=k_a(\bar{p}_c)$;

(2)the static average parameter k_s for pressure distribution along the circumferential direction depends on the downstream pressure $\bar{p}_c$ and the bearing length diameter ratio L/D, or $k_s=k_s(L/D,\bar{p}_c)$;

(3)the static square average parameter k_{sq} for pressure distribution along the circumferential direction depends on the bearing length diameter ratio, or $k_{sq}=k_{sq}(L/D)$;

(4) the average pressure distribution parameters p_m^*, p_m^{**} and p_{qm}^* have no relation with the dimensionless bearing number Λ. Base on the study in Ref. [20], the detail relationship are as follows;

$$k_a=0.31322453\left(1-e^{0.5433077(1-\bar{p}_c)}\right)+0.4$$

$$k_s=1-e^{-0.4924\frac{L}{D}-0.4115\sqrt{\bar{p}_c}}$$

$$k_{sq}=1-e^{-0.9093\frac{L}{D}}$$

Investigations show that it is possible to use these assumptions in the range of the bearing parameters with changes of the bearing number Λ from 1 to 1000, the ratio *L/D* from 0.5 to 2, the ratio of downstream pressure at the supply orifice to the ambient pressure $\bar{p}_c$ from 2.795 to 3.512, $\bar{p}_s$ from 2.026 to 5.974.

5. THE ANALYTICAL FORM FOR OUTPUT PRESSURE OF ORIFICES

From the form of the gas film forces, it is observed that the downstream pressure $\bar{p}_c$ is the key parameter to determine

the characteristic of hybrid gas bearing. So the relation between the supply pressure $\overline{p}_s$ and the downstream pressure $\overline{p}_c$ is critical for establishing the analytical form of the gas film force. In Ref [19], the $\overline{p}_c$ is taken as the structure parameters for hybrid gas bearing, which make the analysis complicated. So the analytical relationship between $\overline{p}_s$ and $\overline{p}_c$ will be derived and help making the supply pressure $\overline{p}_s$ as a structure parameter.

By employing the assumption in Ref [19], the mass flow rate in the axial direction generated from the pressure difference should be equal to that generated from the externally pressurized orifices, $q_{s1} = q_{a1}$

And then,

$$\phi_{orifice} p_s A_{orifice} \sqrt{2} \left(R_0 T_0\right)^{-0.5} \psi_i = \frac{k_L h_m{}^3 p_a^2}{12 \mu R^0 T^0 a} \left(\overline{p}_0^2 - 1\right)$$

From the definition of pressure square average parameter: $\overline{p}_0^2 = k_{sq}\left(\overline{p}_c^2 - 1\right) + 1$:

$$\phi_{orifice} p_s A_{orifice} \sqrt{2} \left(R_0 T_0\right)^{-0.5} \psi_i = \frac{k_L h_m{}^3 p_a^2 k_{sq}}{12 \mu R^0 T^0 a} \left(\overline{p}_c^2 - 1\right)$$

Finally

$$\overline{p}_c = \sqrt{\phi_{orifice} p_s A_{orifice} \sqrt{2} \left(R_0 T_0\right)^{-0.5} \psi_i \frac{12 \mu R^0 T^0 a}{k_L h_m{}^3 p_a^2 k_{sq}} + 1}$$

It indicates that the downstream pressure of bearing clearance can be obtained directly by specifying the supply pressure.

6. THE DYNAMIC CHARACTERISTIC OF HYBRID GAS BEARING

To verify the accuracy of the proposed analytical gas film forces of the hybrid gas bearing, the comparison with the self-acting gas bearing will be carried out first. For the self-acting gas bearing, the model can be obtained by replacing some parameters with constant values. The detail process is as follows:

$\overline{P}_0 = 1$, where $\overline{P}_m = 1$. Take the above equation into the gas film forces, and then the bearing characteristics of self-acting bearing are obtained. The same parameters as Ref [18] are used with different analytical model, where $k_a = 0.5$. Because the clearance of the bearing is divided into eight zones, the parameter $k_L = \pi / 4$.

The dimensionless static stiffness obtained by the proposed model in this paper and by model in Ref [18] is compared in Fig.2, where the bearing length diameter ratio equals to 2.0, 1.5 and 1.0. As the increment of the dimensionless bearing number, the static stiffness of self-acting gas bearing increases. As the rotating angular velocity increases to certain value, the static stiffness with different bearing length diameter ratio goes constant value 1.5. It indicates that the static stiffness increases as the bearing length diameter ratio increases with unchanged rotating speed. As shown in Fig.2, the results obtained by the proposed method agree well with the literature's results.

The attitude angle obtained by the proposed model in this paper and by model in Ref [18] is compared in Fig.3, where the bearing length diameter ratio equals to 2.0, 1.5 and 1.0. As the rotating angular velocity remains small, the attitude angle nearly equals to 90 degree. As the rotating speed increases, the attitude angle decreases. As the rotating speed reach higher enough, the attitude angle comes into 0 degree. So as the increment of the bearing length diameter ratio, the attitude angle decreases, where the rotating speeds keep constant. As shown in Fig.3, the great accuracy between the proposed model and literature model is presented.

The detail data for the comparisons of the stiffness and attitude angle are presented in Tab.2. It indicates that the numerical results of this paper are in good agreement with the reference's results, which make the foundation for the analysis of the gas bearing rotor system.

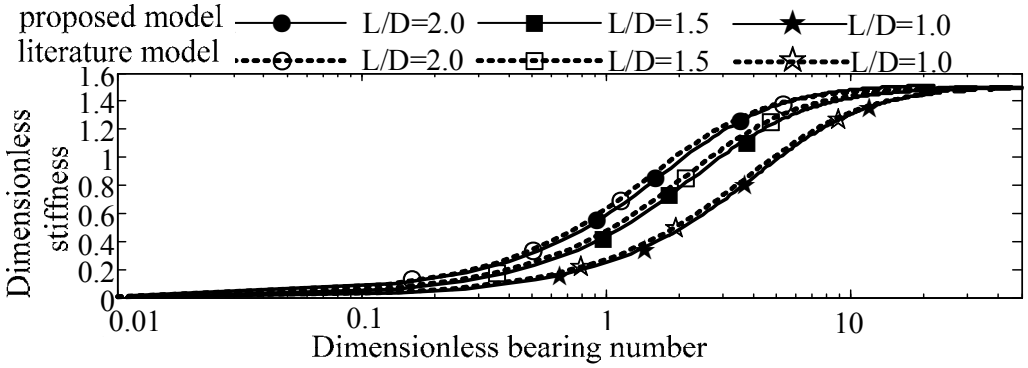

Fig.2 Comparison of dimensionless stiffness for different model varying with bearing numbers

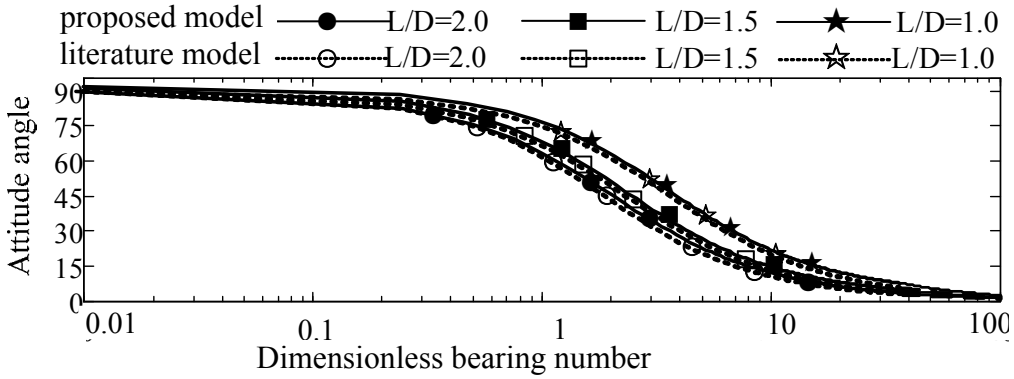

Fig.3 Comparison of attitude angles for different model varying with bearing numbers

Table.2 the comparison of the dimensionless stiffness and attitude angle

Dimensionless bearing number	*L/D=2.0*				*L/D=1.5*				*L/D=1.0*			
	Dimensionless stiffness		Attitude angle		Dimensionless stiffness		Attitude angle		Dimensionless stiffness		Attitude angle	
	In Ref.[18]	In this paper	In Ref.[18]	In this paper	In Ref.[18]	In this paper	In Ref.[18]	In this paper	In Ref.[18]	In this paper	In Ref.[18]	In this paper
0.01	0.0069	0.0068	89.77	89.80	0.0069	0.0068	89.70	89.85	0.0069	0.0068	89.68	89.90
0.2409	0.1675	0.1648	83.64	83.82	0.1205	0.1183	84.01	84.61	0.0667	0.0653	87.48	88.62
1.165	0.7161	0.7132	58.01	58.63	0.5444	0.5438	63.40	64.20	0.3157	0.3120	72.23	73.04
10.4	1.4680	1.4601	10.16	10.29	1.4420	1.4407	12.59	13.08	1.3310	1.3283	19.24	19.80
39.96	1.4980	1.4913	3.25	3.26	1.4960	1.4932	3.34	3.40	1.4860	1.4842	5.19	5.36

The static stiffness of the hybrid gas bearing can be obtained by assuming that $s = 0$. The static stiffness varying with dimensionless bearing number for different supply pressure is acquired in Fig.4. As the dimensionless bearing number increases, the static stiffness increases a little, reaches the peak value and then decreases severely, where the bearing length diameter ratio keeps constant. As the supply pressure increases, the static stiffness gets bigger. The reason for this is as follows: when the dimensionless bearing number remains small, the aerostatic effect plays an important role in the load capacity of hybrid gas bearing, which generates most of the stiffness; as the bearing number increases, the aerodynamic effect raises the stiffness; as the bearing number reaches big enough, the aerodynamic effect suppresses the aerostatic effect, which attenuates the stiffness. When the dimensionless bearing number reaches nearly 1000, the stiffness mainly generates from the aerodynamic effect, so the supply pressure has nearly no influence on the static stiffness.

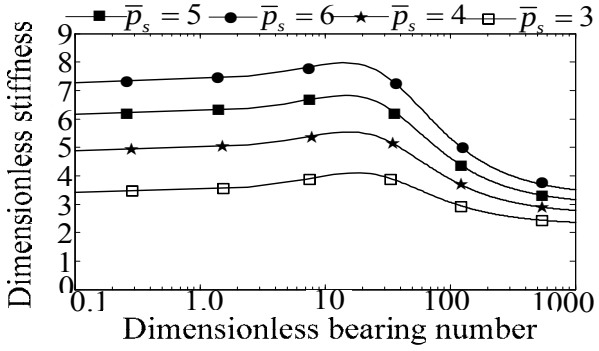

(a) $L/D = 0.5$

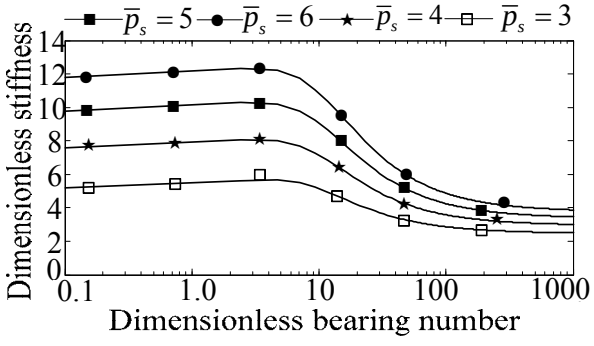

(b) $L/D = 1.0$

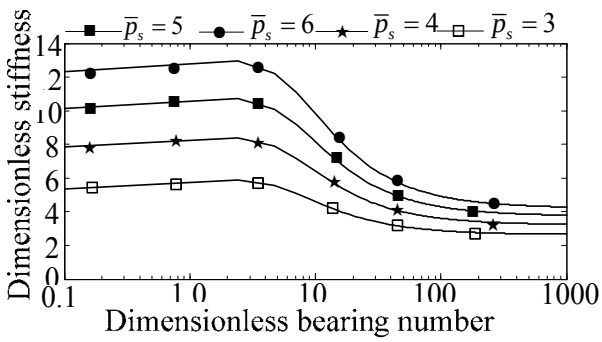

(c) $L/D = 1.5$

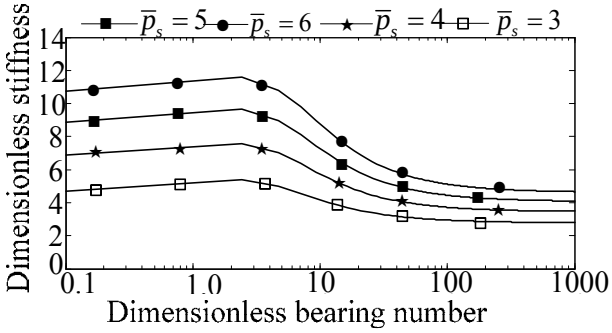

(d) $L/D = 2.0$

Fig.4 the dimensionless stiffness varying with dimensionless bearing number for different supply pressure

The static stiffness varying with dimensionless bearing number for different bearing length diameter ratio *L/D* is acquired in Fig.5. It is observed that the variation of the *L/D* does not affect the total tendency of the static stiffness: As the dimensionless bearing number increases, the static stiffness increases a little, reaches the peak value and then decreases severely. As the supply pressure equals to 6.0, and dimensionless bearing number is smaller than 5, the static stiffness of *L/D* equaling 1.5 is the biggest, whereas that of *L/D* equaling 2.0 is smaller, that of *L/D* equaling 1.0 is the smallest. The static stiffness of the hybrid bearing with the supply pressure of 4.0 has the same trend as that with the supply pressure of 6.0, whereas the amplitude is smaller. So it can be concluded that the bearing with bigger length diameter ratio *L/D* may not have bigger static stiffness when the supply pressure remain constant. As the dimensionless bearing number comes into high, the length diameter ratio has little influence on the stiffness.

The dynamic coefficients varying with bearing length diameter ratio for supply pressure equaling to 6.0 and bearing number of 5.27 are presented in Fig.6. It is observed that the dimensionless coupling stiffness K_{xy} increases and then decreases, as the dimensionless frequency decreases in Fig.6 (a). In Fig.6 (b), the dimensionless damping coefficients are negative. The amplitude of the coupling damping with *L/D* of 2.0 is the biggest for the case that dimensionless frequency is smaller than 0.2. As the frequency becomes bigger than 0.2, the amplitude of the coupling damping coefficients with *L/D* of 1.0 is the biggest. The damping coefficients become zero as the increments of the frequency with different bearing length diameter ratio. As shown in Fig.6 (c), the dimensionless direct stiffness increases first and then attenuates as the dimensionless frequency increases, and reaches the peak value with frequency of 1.0. The difference of the direct stiffness between different bearing diameter ratios becomes obvious. It indicates that the direct damping coefficients C_{yy} increases to positive value and then decrease to negative value, finally comes into zero in Fig6.(d). As the dimensionless frequency remains small, the direct damping coefficients with *L/D* of 2.0 are the biggest; those with *L/D* of 1.5 are smaller; and those with *L/D* of 0.5 are smallest. As the increment of the dimensionless frequency, the direct damping coefficients become negative, and the difference between coupling damping with different bearing length diameter ration comes into negligible.

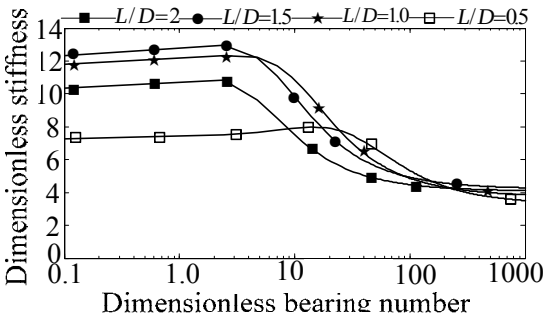

(a) $\bar{p}_s = 6.0$

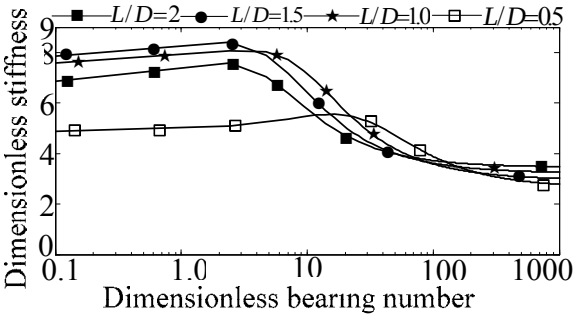

(b) $\bar{p}_s = 4.0$

Fig.5 the dimensionless stiffness varying with dimensionless bearing number for different *L/D*

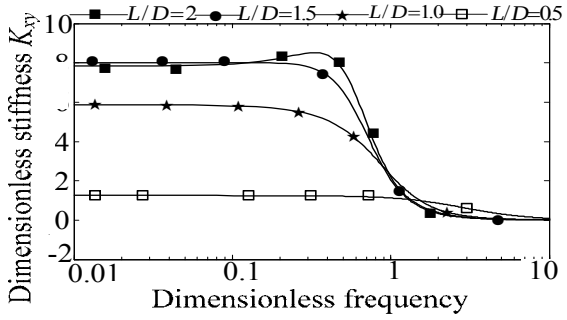

(a)coupling stiffness

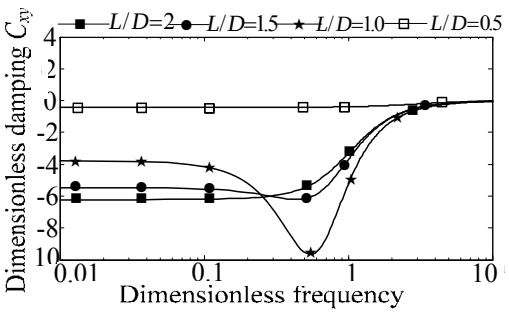

(b)coupling damping

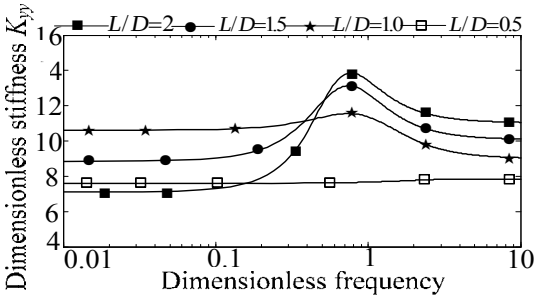

(c)direct stiffness

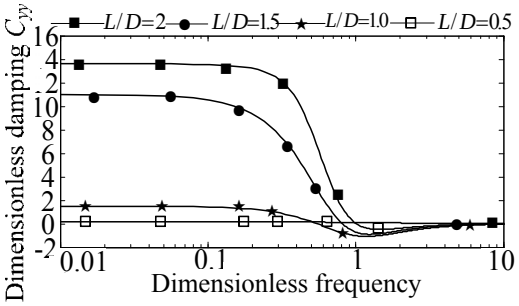

(d)direct damping

Fig.6 the dynamic coefficients varying with bearing length diameter ratio for supply pressure equaling to 6.0 and bearing number of 5.27

CONCLUSION

The flow in the hybrid gas journal bearing is depicted by the transfer function in this paper, and the gas film force of hybrid gas bearing is derived by analytical form. Based on the original work in the literature, a more generalized means for deducing procedure is carried out. The downstream pressure of bearing clearance at the orifice can be obtained directly by employing the supply pressure with the developed method. By using the Laplace transform the dynamic coefficients with frequency as variations are acquired, which provide a reliable and effective method to analyze the static and dynamic characteristics of eight orifices hybrid gas bearing.

Based on the proposed analytical method, the influence of bearing length diameter ratio, supply pressure and the bearing number on static and dynamic characteristics is presented. It indicates that when the dimensionless bearing number remains small, the aerostatic effect play an important role in the load capacity of hybrid gas bearing, which generates most of the stiffness; as the bearing number increases, the aerodynamic effect raises the stiffness; as the bearing number increases to a certain value, the aerodynamic effect suppresses the aerostatic effect, which attenuates the stiffness. For the cases of dynamic coefficients, as the bearing number keep constant, the variation of bearing length diameter ratio does not only affect the amplitude of the dynamic coefficients, but also affect the distribution laws for the coefficients that vary with the excited frequency.

ACKNOWLEDGEMENT

The research presented here was supported by " the Fundamental Research Funds for the Central Universities" (Grant No. HIT. NSRIF. 20100028). The authors are grateful for the support.

REFERENCES

[1]Pan C, Sternlicht B., 1961, “On the Translatory Whirl Motion of a Vertical Rotor in Plain Cylindrical Gas-Dynamic Journal Bearings,” NP-10394, General Electric Co. General Engineering Lab, Schenectady, NY.

[2]Rentzepis GM, Sternlicht B., 1962, “On the Stability of Rotors in Cylindrical Journal Bearings,” Journal of Basic Engineering., 84(3), pp.521-532.

[3]Ausman JS., 1963, “Linearized Ph Stability Theory for Translatory Half-Speed Whirl of Long Self-Acting Gas-Lubricated Journal Bearings,” Journal of Basic Engineering. 83, pp.611-619.

[4]Castelli V, Elrod HG, 1965, “Solution of the Stability Problem for 360 Deg Self-Acting, Gas-Lubricated Bearings,” Journal of Basic Engineering, 87(1), pp. 199-212.

[5]Lund JW., 1968, “Calculation of Stiffness and Damping Properties of Gas Bearings.” Journal of Lubrication Technology, 90, pp.793-801.

[6]Lund JW. , 1976, “Linear Transient Response of a Flexible Rotor Supported in Gas-Lubricated Bearings,” ASME Journal of Lubrication Technology,98(1), pp.57-65.
[7] Carpino, M. and G. Talmage .,2006, "Prediction of rotor dynamic coefficients in gas lubricated foil journal bearings with corrugated sub-foils." Tribology transactions 49(3),pp.400-409.
[8] LE LEZ, S. and M. ARGHIR, et al. ,2007, "Static and dynamic characterization of a bump-type foil bearing structure." Journal of tribology 129(1): pp.75-83.
[9] San Andres, Luis., 1995, “Turbulent Flow Foil Bearings for Cryogenic Applications,” ASME Journal of Tribology, 117(1) pp. 185-195.
[10] Lee, N. S., Choi, D. H., Lee, Y. B., Kim, T. H. and Kim, C. H. , 2002, “The Influence of the Slip Flow on Steady-State Load Capacity, Stiffness and Damping Coefficients of Elastically Supported Gas Foil Journal Bearings,” Tribology Transactions, 45, pp 478-484.
[11 Faria, M. and L. San Andres ,2000, "On the numerical modeling of high-speed hydrodynamic gas bearings." Journal of tribology 122(1), pp.124-130.
[12] Morosi, S. and I. Santos (2009). "Modeling of Hybrid Permanent Magnetic-Gas Bearings." 20th International Congress of Mechanical Engineering, ABCM, Gramado -RS, Brazil.
[13] Castelli V, Elrod H G., 1961, “Solution of the stability problem for 360 degree self-acting, gas-lubricated bearing,” ASME Journal of Basic Engineering. 87(1), pp. 199 – 212.
[14]Castelli V, Stevenson C H., 1967, “A semi-implicit numerical method for treating the time transient gas lubrication equation,” New York, Mechanical Technology Inc, TID-23853.
[15] Dimofte F., 1992, “Fast methods to numerically integrate the Reynolds equation for gas fluid films,” New York, NASA Technical Memorandum, 105415.
[16] Bou-sa B, Grau G, Iordanoff I., 2008, “On Nonlinear rotor dynamic effects of aerodynamic bearings with simple flexible Rotors,” Journal of Engineering for Gas Turbines and Power, 130(1), 012503.
[17] Wang Chengchi, Jang Mingjyi, Yeh Yenliang., 2007, “ Bifurcation and nonlinear dynamic analysis of a flexible rotor supported by relative short gas journal bearings,” Chaos, Solitons and Fractals, 32(2), pp.566-582.
[18] Belforte G, Raparelli T, Viktorov V., 2002, “Modeling and Identification of Gas Journal Bearings: Self-Acting Gas Bearing Results,” Journal of Tribology, 124(4), pp.716-724.
[19] Viktorov V, Belforte G, Raparelli T., 2005, “ Modeling and Identification of Gas Journal Bearings: Externally Pressurized Gas Bearing Results,” Journal of Tribology, 127(3), pp.548-556.
[20]Liu Zhan Sheng, Zhang Guang Hui and Xu Huai Jin.,2009, “Performance analysis of rotating externally pressurized air bearings,” Proceedings of the Institution of Mechanical Engineers, Part J: Journal of Engineering Tribology, 223(4), pp.653-663.